Stem Cell Reports
Article
OPEN ACCESS

Reversal of Cellular Phenotypes in Neural Cells Derived from Huntington's Disease Monkey-Induced Pluripotent Stem Cells

Richard L. Carter,[1,2,3] Yiju Chen,[1,2] Tanut Kunkanjanawan,[1,4] Yan Xu,[1,2] Sean P. Moran,[1,2] Kittiphong Putkhao,[1,4] Jinjing Yang,[1,2] Anderson H.C. Huang,[5] Rangsun Parnpai,[4] and Anthony W.S. Chan[1,2,3,*]

[1]Yerkes National Primate Research Center, Atlanta, GA 39329, USA
[2]Department of Human Genetics, Emory University School of Medicine, Atlanta, GA 30322, USA
[3]Genetics and Molecular Biology Program, Emory Laney Graduate School, Atlanta, GA 30322, USA
[4]Embryo Technology and Stem Cell Research Center, School of Biotechnology, Suranaree University of Technology, Nakhon Ratchasima 30000, Thailand
[5]Department of Oral Pathology, School of Dentistry, Kaohsiung Medical University, Kaohsiung 807, Taiwan, Republic of China
*Correspondence: awchan@emory.edu
http://dx.doi.org/10.1016/j.stemcr.2014.07.011

SUMMARY

Huntington's disease (HD) is a dominant neurodegenerative disorder caused by the expansion of glutamine residues in the N-terminal region of the huntingtin (HTT) protein. The disease results in progressive neuronal loss, leading to motor, cognitive, and psychiatric impairment. Here, we report the establishment of neural progenitor cell (NPC) lines derived from induced pluripotent stem cells (iPSCs) of transgenic HD monkeys. Upon differentiation to neurons, HD neural cells develop cellular features of HD, including the formation of nuclear inclusions and oligomeric mutant HTT (mHTT) aggregates, as well as increased apoptosis. These phenotypes are rescued by genetic suppression of HTT and pharmacological treatment, demonstrating the ability of our HD cell model to respond to therapeutic treatment. The development and reversal of HD-associated phenotypes in neural cells from HD monkeys provides a unique nonhuman primate (NHP) model for exploring HD pathogenesis and evaluating therapeutics that could be assessed further in HD monkeys.

INTRODUCTION

Huntington's disease (HD) is an autosomal dominant neurodegenerative disorder caused by the expansion of CAG repeats in the coding region of the huntingtin (*HTT*) gene *IT15* (MacDonald et al., 1993). The mutation produces an extended stretch of glutamine residues spanning the N terminus of the HTT protein. Aggregation of oligomeric mHTT fragments and the formation of nuclear inclusions have been identified as hallmarks of the disease (DiFiglia et al., 1997); however, the role of mHTT aggregation in neurodegeneration remains unclear (Arrasate et al., 2004). Advances in cellular reprogramming techniques have led to broad applications for induced pluripotent stem cells (iPSCs) derived from patients as a model to recapitulate disease conditions because they share identical genetic defects with patients (Grskovic et al., 2011). Recent studies on iPSCs derived from HD patients have shown promise as possible HD models (An et al., 2012; Camnasio et al., 2012; Cheng et al., 2013; HD iPSC Consortium, 2012; Zhang et al., 2010). As these studies reveal the potential for pluripotent HD stem cell models as a tool for drug discovery and therapeutic development, the need arises for a preclinical nonhuman primate (NHP) model of HD that will be ready to assess the safety and efficacy of new therapeutics (Emborg et al., 2013; Perrier and Peschanski, 2012). Because safety concerns limit the direct translation of findings from human HD iPSC studies, HD monkey models provide a unique platform for long-term in vivo assessments, especially in the case of genetic correction and cell therapies. Here, we report the derivation of NPCs from HD monkey iPSCs. The resulting HD-NPCs are capable of differentiating into neural cells and develop classic HD cellular phenotypes. Furthermore, both genetic and pharmacologic treatments could reverse HD phenotypes in HD neural cells. HD monkeys and their derivative iPSCs provide an unprecedented opportunity for assessing personal medicine in higher primates, and HD-NPCs are a unique cellular platform for studying HD pathogenesis and evaluating drug efficacy.

RESULTS

Monkey NPCs Generate GABA$^+$ Neurons following In Vitro and In Vivo Neural Differentiation

HD monkey dental pulp stromal cells (DPSCs) and fibroblasts were reprogrammed by introducing rhesus genes encoding *OCT4*, *SOX2*, and *KLF4* through retroviral gene transfer following protocols described in our previous report (Chan et al., 2010; Snyder et al., 2011). HD-iPSC lines (HD-3 and HD-14) were generated from two HD monkeys. HD-2 was embryonic stem cells (ESCs) derived from transgenic embryos from an HD monkey (Putkhao et al., 2013) (Table S1 available online). HD cell lines express exon 1 of the human *HTT* and green fluorescent protein

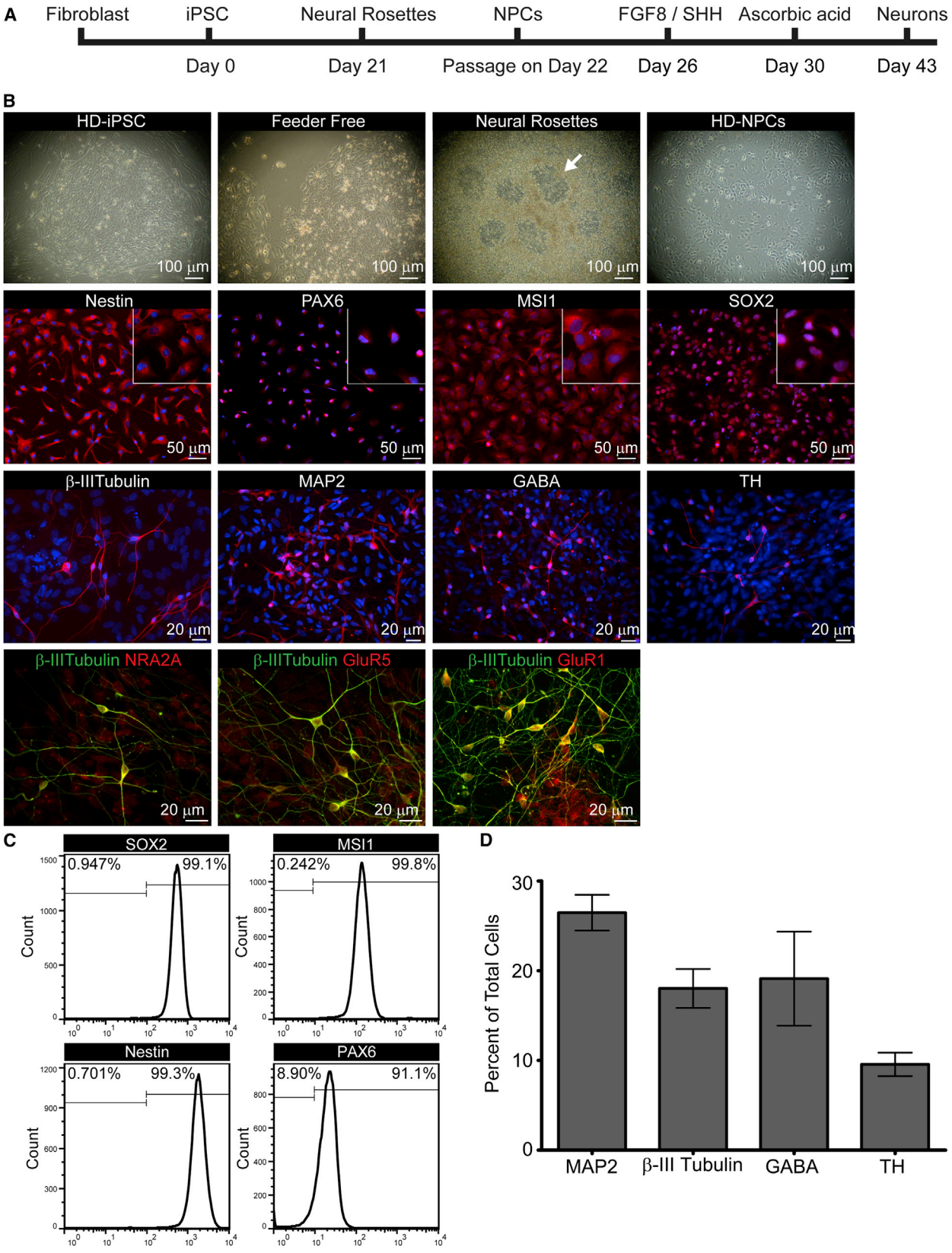

(legend on next page)

(*GFP*) genes under the control of the human polyubiquitin-C promoter (*UBC*) (Figure S1). HD-2, HD-3, and HD-14 lines carried CAG repeat sizes of 29, 72, and 27/65, respectively. Wild-type (WT) cells lines (WT-2, WT-14, and WT-28) were generated from nontransgenic wild-type control monkeys derived from ESCs (WT-2 and WT-28) or by cellular reprogramming (WT-14) (Table S1). Stem cell lines expressed pluripotent stem cell markers, including OCT4, SSEA4, Tra-1-60, and alkaline phosphatase (Figure S1). In addition, cytogenetic analysis revealed a normal diploid karyotype matching gender to that of the HD monkey donor (Figure S1) (Chan et al., 2010; Putkhao et al., 2013).

To overcome technical hurdles associated with long-term stem cell culture, we derived stable NPC lines from HD monkey pluripotent stem cells (Figure 1A). NPCs displayed ectodermal rosette-like structures and exhibited characteristic NPC morphology after monolayer culture (Figure 1B). NPC populations were expandable for over 30 passages and could be frozen and thawed with high viability and maintain neural differentiation competency. NPCs expressed canonical neural precursor markers, including Nestin, PAX6, Musashi 1 (MSI1), and SOX2, confirmed by immunocytochemistry and quantitative RT-PCR (qRT-PCR) (Figures 1B and S2). Homogeneity of NPCs was confirmed by fluorescence-activated cell sorting (FACS) analysis (Figure 1C and Table S2). These results showed the successful establishment of HD- and WT-NPCs at high homogeneity that can be used for in vitro derivation of neural cells.

To determine that HD-NPCs were capable of differentiating into neuronal cell types, HD-NPCs were cultured for 21 days on polyornithine/laminin (P/L)-coated glass slides with neural differentiation medium (Figure 1A). Neurons derived from HD-NPCs expressed structural neural markers, microtubule-associated protein (MAP2, 27%), and β-III tubulin (18%), as well as neurotransmitter markers γ-aminobutyric acid (GABA, 21%) and tyrosine hydroxylase (TH, 10%), as demonstrated by immunostaining using specific antibodies (Figures 1B and 1D). β-III tubulin-positive neurons derived from HD-NPCs also stained positive for neural receptor subunits, including NR2A, GluR1, and mGluR5 (Figure 1B).

We further assessed neural differentiation potential for HD-NPCs in vivo. WT-2 and HD-14 NPCs were transplanted into the striatum of 10-week-old SCID mice. Although HD-NPCs carry both *mHTT* and *GFP* transgenes, WT-NPCs were introduced with lentivirus expressing *GFP* gene under the control of the *UBC* promoter for identification. At 12.5, 15, and 16 weeks posttransplantation, the brains of the transplanted mice were sectioned and stained for neuronal markers. Confocal imaging revealed that GFP-positive WT-2 and HD-14 grafts were also positive for neuronal markers DCX (Figures 2A and 2B), GABA (Figures 2C and 2D), and striatal neuron marker DARPP-32 (Figures 2E and 2F). At 12.5 weeks, WT-2 neurons showed positive staining for neuronal marker NeuN (Figure 2I). NeuN-positive HD-14 neurons were seen after 16 weeks (Figure 2J), suggesting that neural differentiation and maturation may possibly be impacted by mHTT in HD cells.

Immunostaining with mEM48, an antibody reactive to mHTT with expanded glutamine repeats (Chan et al., 2010), revealed grafted cells positive for mHTT inclusions (Figures 2G and 2H). WT and HD-NPCs were also capable of generating glial cells as indicated by positive GFAP staining (Figures 2K and 2L). These results show that iPSC-derived HD-NPCs survived after xenograft in the striatum and were capable of differentiating into striatal $GABA^+$ neurons both in vitro and in vivo.

Expression of mHTT and Formation of Intranuclear Inclusions during Neural Differentiation

The aggregation of mHTT and the formation of intranuclear inclusions are classic HD-associated neuronal phenotypes (DiFiglia et al., 1997) that have been described in humans as well as animal models (Wang et al., 2008; Yang et al., 2008). Although HTT expresses in all cell types, neuronal cell types are most susceptible to the toxicity caused by mHTT (Johnson and Davidson, 2010). qRT-PCR analysis of HD-NPCs during neural differentiation revealed elevated expression of total *HTT* transcripts in HD neural cells compared to WT neurons (Figure 3A). Western blot analysis of HD and WT cells at different stages of differentiation revealed increased accumulation of oligomeric mHTT in HD-3 and HD-14 (Figure 3B). Interestingly, the

Figure 1. Derivation of HD-NPCs from iPSCs and In Vitro Neural Differentiation of HD-NPCs

(A) Schematic diagram depicting NPC and neuron derivation from rhesus macaque iPSCs.

(B) Bright-field image of HD-14 NPCs at progressing stages of differentiation. Arrows indicate neural rosettes (first row). Immunocytochemistry of HD-14 NPCs stained for Nestin, PAX6, MSI1, and SOX2 (red; second row). HD-14 in vitro differentiated neurons stained for β-III tubulin, MAP2, GABA, and TH (red; third row). Neural receptor subunits are expressed in HD neural cells; NR2A (red), GluR1 (red), and mGlur5 (red) colabeled with β-III tubulin (green) (fourth row). Nuclear staining is shown using Hoechst (blue).

(C) FACS analysis of HD-14 NPCs using antibodies for NPC markers. FACS data for all cell lines are listed in Table S2.

(D) Quantification of neurons derived from in vitro differentiated NPCs. Error bars indicate the SEM. Data represent three biological replicates.

See also Figures S1 and S2 and Table S2.

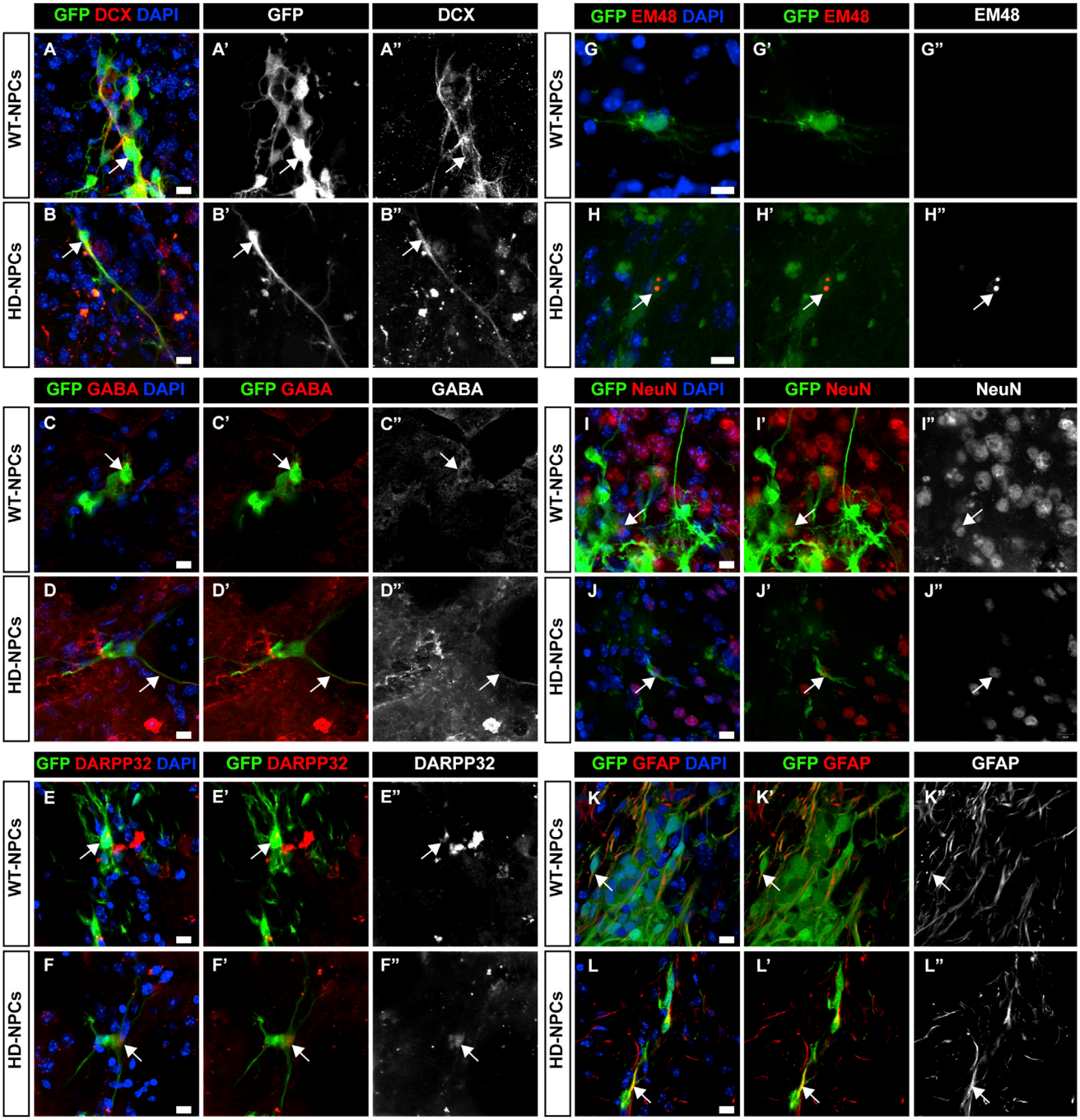

Figure 2. Characterization of Neuron Differentiation in Grafted NPCs

(A and B) Twelve and a half weeks posttransplantation, WT and HD cell grafts were positive for DCX (red).

(C and D) Fifteen weeks posttransplantation, WT and HD cell grafts were positive for GABA (red).

(E and F) Fifteen weeks posttransplantation, WT and HD cell grafts were positive for DARPP32 (red).

(G and H) Sixteen weeks posttransplantation, WT cell grafts were negative for mEM48; HD cell grafts show colocalization of GFP (green) and mEM48-positive nuclear inclusions (red).

(I and J) Twelve and a half weeks posttransplantation, WT cell grafts express neuronal marker NeuN (red). NeuN-positive HD cell grafts were observed after 16 weeks grafting (red).

(K and L) WT and HD cell grafts differentiate to glial cells indicated by positive GFAP staining (red).

Arrows indicate marker-positive transplanted neurons. Scale bars, 10 μm.

increased oligomeric aggregates are only seen in HD neural cells and are undetectable in HD-iPSCs. Immunostaining using mEM48 revealed the development of HTT aggregates and intranuclear inclusions in differentiated HD neurons colabeled with neuronal markers DCX, MAP2, and GABA (Figure 3C).

In addition to the development of classic HD cellular phenotypes, we also investigated whether HD-NPCs were more susceptible to oxidative stress compared to WT-NPCs, as previously shown in human HD-iPSCs and neurons (An et al., 2012; HD iPSC Consortium, 2012). Hydrogen peroxide (H_2O_2) was supplemented into culture medium to induce oxidative stress. TUNEL assay following H_2O_2 incubation demonstrated a significant increase in cell death in HD-NPCs compared to WT-NPCs (Figures 3D and 3E; $p < 0.01$). This observation was further supported by flow cytometric analysis of caspase 3/7 activity, which revealed a significant increase in apoptotic cells in HD-NPCs compared to WT-NPCs following exposure to H_2O_2 (Figure 3F; $p < 0.01$). Together, these findings show that HD neural cells mirror key cellular phenotypes associated with mHTT.

Reversal of HD-Associated Phenotypes by RNAi and Memantine

Following the characterization of HD phenotypes in neural cells derived from HD monkeys, we investigated whether these phenotypes could be rescued by therapeutic treatment. RNAi-mediated reduction of HTT in HD models has shown promise in a number of studies (Boudreau et al., 2009; McBride et al., 2011). We postulated that reducing the expression of HTT in HD-NPCs would confer a therapeutic benefit. HD-NPCs were infected with a lentivirus expressing small hairpin RNA (shRNA) targeting the *HTT* transcript. After Zeocin selection to establish stable transformed NPC lines, qRT-PCR analysis showed that *HTT* expression in shRNA-treated NPCs (shHD-3 and shHD-14) was reduced by approximately 50% (Figure 4A; $p < 0.05$). Furthermore, oligomeric HTT aggregation was reduced in shHD-3 and shHD-14 as revealed by western blot using mEM48 antibody (Figure 4B; top panel). Slight reduction of soluble HTT detected by 1C2 antibody was also observed in cells treated with shRNA-HTT (Figure 4B; lower panel). We next determined whether the reduction of HTT could reduce apoptosis in HD-NPCs. shHD-3 and HD-3 NPCs were challenged with H_2O_2 to induce oxidative stress. As demonstrated by caspase 3/7 assay, the percentage of apoptotic cells was significantly reduced in shHD-3 NPCs in comparison to HD-3 NPCs (Figure 4C; $p < 0.01$). Next, we performed TUNEL assay to assess cell death in shHD-3 and shHD-14 neural cells following differentiation. In correlation with our caspase assay, we observed a significant reduction of apoptotic neural cells that had reduced *HTT* expression compared to HD neural cells not expressing shRNA (Figure 4D; $p < 0.05$).

In addition to mHTT expression, neurodegeneration has been attributed to *N*-methyl-D-aspartate receptor (NMDAR)-mediated cytotoxicity in HD (Marco et al., 2013). Reports of using memantine, a well-characterized NMDAR antagonist, have shown some promise as a potential therapy for HD (Milnerwood et al., 2010). To test whether treatment with memantine could rescue the cell death observed in HD neurons, 10 μM memantine was supplemented into neural differentiation medium 24 hr prior to assessing cytotoxicity. The cytotoxicity of HD neurons treated with memantine was significantly reduced compared to untreated HD neurons, whereas there was no significant change in cytotoxicity in WT neurons (Figure 4E; $p < 0.01$). Together, these results show that HD monkey neural cells respond to potential therapeutic treatments, suggesting our model will be useful as a platform for drug assessment.

DISCUSSION

This study reports the development of an HD-NPC model derived from the iPSCs of HD NHPs. We established stable and expandable NPC lines from HD monkeys that are capable of neural differentiation in vitro and in vivo. HD neural cells develop classic cellular phenotypes of HD that could be reversed using both genetic and pharmacological treatments. Though efforts to differentiate iPSCs or directly differentiate somatic cells to target cells of interest are ongoing, establishing potent NPC lines from iPSCs provides an advantage by allowing easy maintenance of a progenitor cell population committed to the neuronal lineage, thus enhancing homogeneity in subsequent neural differentiation (Koch et al., 2009). Such HD-NPC lines are important for in vitro neural differentiation for drug discovery research, whereas competency in in vivo differentiation is important for cell replacement therapy.

In vitro differentiation methods used in this system were similar to protocols described for human iPSC neural differentiation, resulting in neurons positive for GABA, TH, and mature neural markers. NPC grafts after in vivo differentiation were positive for glial marker GFAP and mature neural markers; however, we noticed that survival of NPCs and derivative neural cells at the graft site was more impaired in HD-NPCs compared to the contralateral side implanted with WT-NPCs. A possible explanation for this observation is that only 50,000 NPCs were grafted into the mouse striatum. This number is relatively low compared to other studies that grafted over 100,000 cells (Nicholas et al., 2013; Nori et al., 2011). Furthermore, in this study NPCs were transplanted as a single cell suspension, potentially leading to reduced survival of cell grafts compared to other

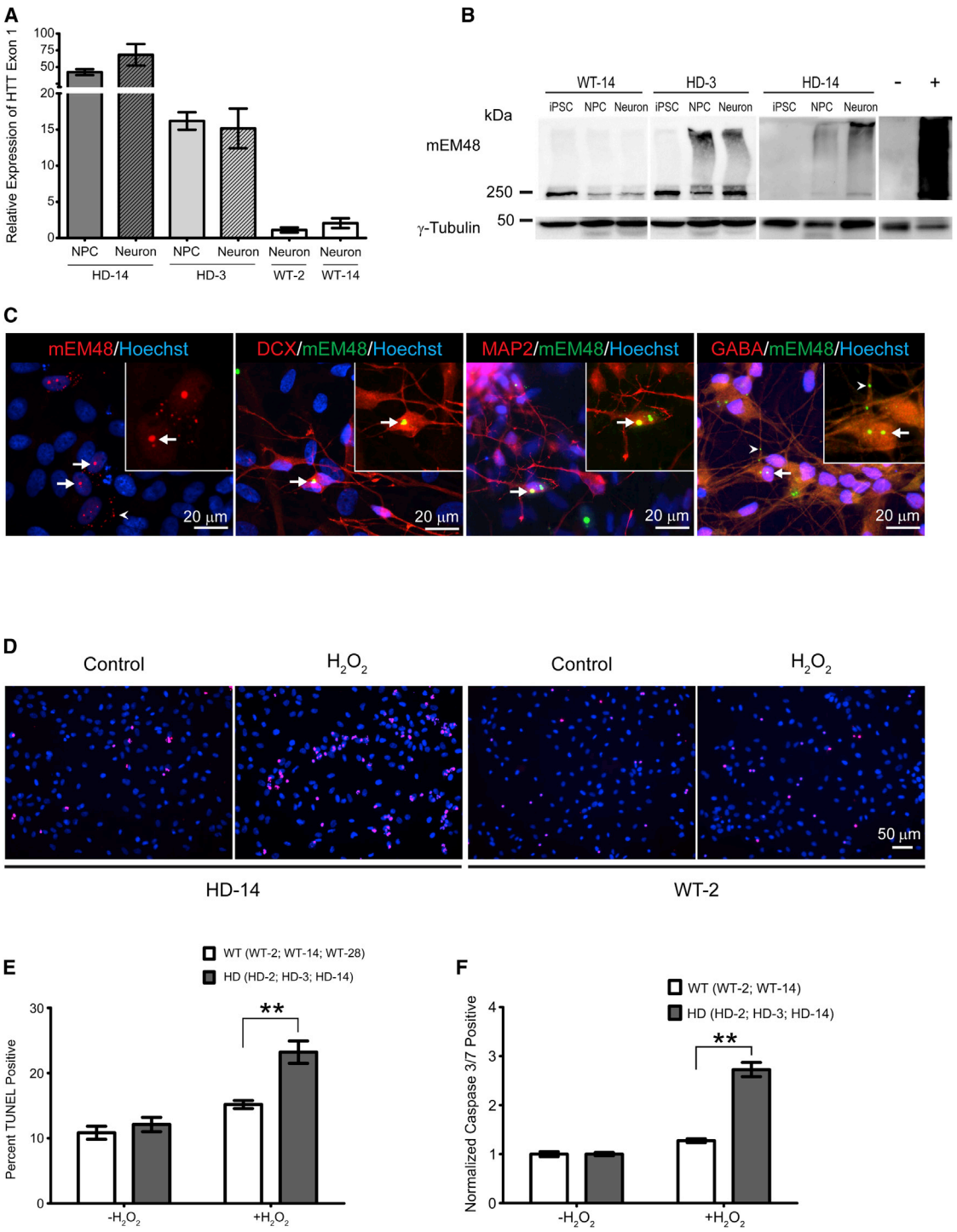

Figure 3. Elevated Expression and Aggregation of mHTT Accompany Increased Vulnerability to Oxidative Stress in HD Cells

(A) qRT-PCR analysis of *HTT* exon 1 during in vitro neural differentiation. Expression levels are compared to WT-2 neuron control line. Results were from three biological replicates. qRT-PCR samples run in duplicate. Data and error bars are represented as mean ± SEM.

(B) Western blot analysis revealed an increase in oligomeric mHTT that correlates with neuronal differentiation stage. Notice aggregate accumulation in the stacking gel (above 250 kDa). Negative (−) and positive (+) lanes are frontal cortex samples from nontransgenic and HD monkeys, respectively.

(legend continued on next page)

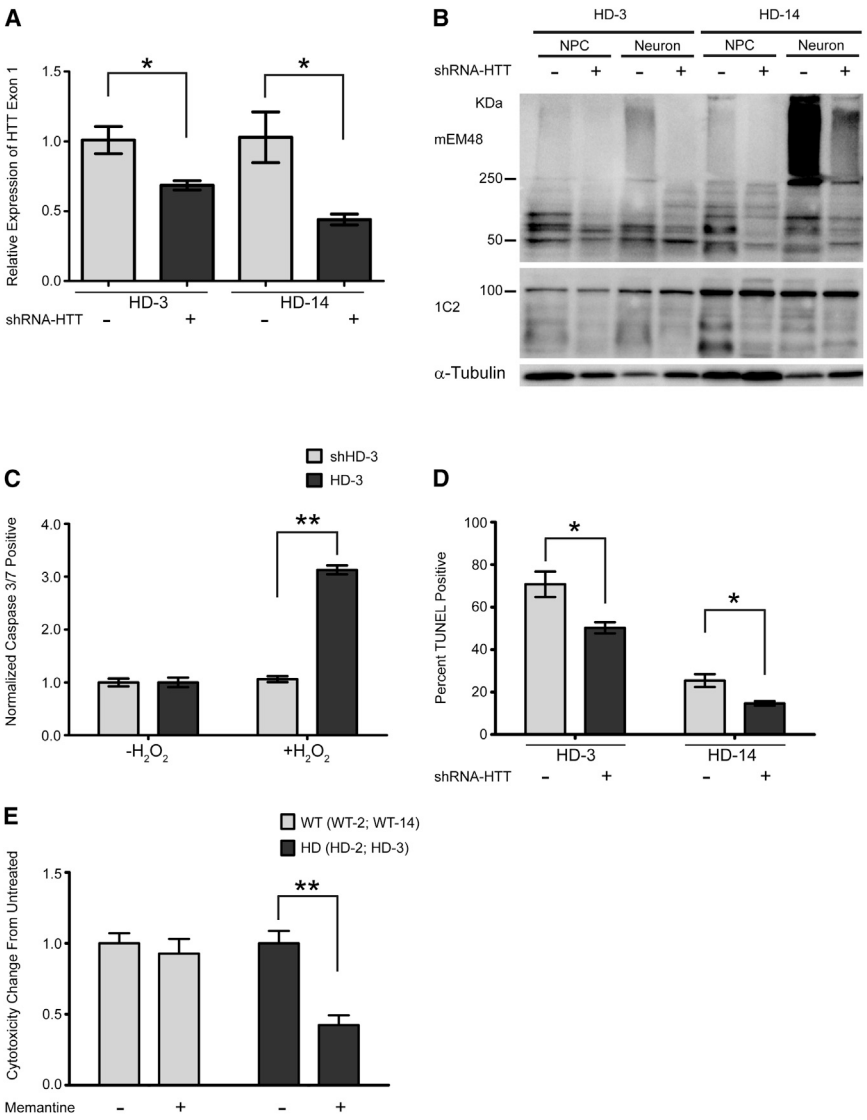

Figure 4. Reversal of HD-Associated Phenotypes Using shRNA and Memantine

(A) qRT-PCR analysis of *HTT* exon 1 expression in HD-3 and HD-14 NPCs after infection with lentivirus expressing shRNA-HTT. Results shown from three biological replicates, qRT-PCR samples run in duplicate. Data and error bars are represented as mean ± SEM (*$p < 0.05$, ANOVA).

(B) Western blot analysis of mHTT aggregation in HD-3 and HD-14 NPCs and in vitro differentiated neural cells with (+) or without (−) expressing shRNA-HTT.

(C) Quantification of caspase 3/7-positive HD-3 and shHD-3 NPCs following H_2O_2 exposure. Values represent fold change from untreated sample. Results are shown from three biological replicates. Data and error bars are represented as mean ± SEM (**$p < 0.001$, ANOVA).

(D) Quantification of TUNEL assay on HD-3 and HD-14 neurons after in vitro differentiation with or without expressing shRNA-HTT. Percentage of TUNEL-positive cells calculated from total number of cells identified by Hoechst staining. Results are shown from three biological replicates. Data and error bars are represented as mean ± SEM (*$p < 0.05$, ANOVA).

(E) Cytotoxicity profile of neurons treated with 10 μM memantine drug measured by G6PD assay. Values represent mean fold change in cytotoxicity from untreated cells. Cytotoxicity values averaged from two HD lines (HD-2, HD-3) and two WT lines (WT-2, WT-28) from three repeated experiments. Data and error bars are represented as mean ± SEM (*$p < 0.05$, ANOVA).

transplantation studies that graft neurospheres (Nori et al., 2011). Together, these results cohere with our findings that the progressive increase in mHTT expression and the accumulation of oligomeric mHTT in neural differentiating HD-NPCs, combined with reduced tolerance to oxidative stress, result in a higher apoptotic rate and increased cell death.

As a potential platform to model HD cellular pathogenesis, an important goal of this study was to assess whether

(C) Left: staining of in vitro differentiated HD-NPCs with mEM48 (red) reveals distinct intranuclear inclusions and cytosolic aggregates (arrowhead) of mHTT. Middle left: mHTT inclusions (green) colabeled with DCX (red). Middle right: mHTT inclusions (green) colabeled with MAP2 (right; red). Right: mHTT inclusions and neuropil aggregates (arrowhead; green) colabeled with GABA (red). Staining using Hoechst (blue). Arrows indicate intranuclear inclusions.

(D) Images represent TUNEL staining of WT-2 and HD-14 NPCs after 24 hr H_2O_2 challenge. H_2O_2 TUNEL-positive cells (red). Nuclear staining is shown using Hoechst (blue).

(E) Quantification of TUNEL assay on HD- and WT-NPCs following H_2O_2 exposure. TUNEL-positive cell (percentage) was averaged for three HD lines (HD-2, HD-3, HD-14) and three WT lines (WT-2, WT-14, WT-28). Percentage of TUNEL-positive cells was calculated from total number of cells from three biological replicates of each cell line. Data are represented as mean ± SEM (**$p < 0.001$, ANOVA).

(F) Quantification of caspase 3/7-positive HD-NPCs compared to WT-NPCs following H_2O_2 exposure. Apoptotic population percentage was averaged for three HD lines (HD-2, HD-3, HD-14) and two WT lines (WT-2, WT-14). Values represent fold change from untreated sample. Results are shown from three biological replicates of each cell line. Data and error bars are represented as mean ± SEM (**$p < 0.001$, ANOVA).

our cellular model recapitulates disease-associated pathologic events. We found that an increase of intranuclear inclusions and the accumulation of oligomeric, soluble, and insoluble mHTT aggregates were correlated with neuronal differentiation. This observation mirrors a key neural pathology seen in HD patients' brains, as well as in HD monkey models (DiFiglia et al., 1997; Yang et al., 2008). In addition to mHTT aggregation, HD-NPCs show increased apoptosis induced by exposure to H_2O_2 as a means of inducing oxidative stress. This disease-dependent difference in vulnerability to exogenous stress recapitulates phenotypes characterized by various studies using human pluripotent stem cells (HD iPSC Consortium, 2012). These findings suggest that our in vitro system is comparable to other previously described cellular models using HD-NPCs, and derivative neural cells develop pronounced HD cellular phenotypes. Furthermore, these HD phenotypes develop independent of treatment with proteasome inhibitors, which in some reports were necessary to induce HD-associated phenotypes (Cheng et al., 2013). We suspect that, unlike human iPSCs, our HD-NPCs express multiple copies of the truncated *mHTT* gene with an expanded polyglutamine tract regulated by the *UBC* promoter, which may lead to more dramatic phenotypes and impact neural differentiation.

The capability of HD monkey neural cells to respond to in vitro drug and gene therapy provides a proof of principle that this cellular model of HD could make a powerful resource for the assessment and development of candidate therapeutic strategies. By using an RNAi approach to reduce HTT expression and by treating neurons with memantine, we were able to ameliorate cell death phenotypes. With this result, we show the potential utility of our system for screening therapeutic targets in HD, with the important bonus that our model provides a unique opportunity for future assessments in HD monkeys in vivo. Furthermore, reports describing the successful transplantation and integration of monkey neural progenitors into targeted brain regions of NHPs (Emborg et al., 2013; Hashimoto et al., 2012) point to the feasibility of cell replacement studies in NHP models of neurodegenerative disease. These reports, combined with our recent success in developing HD monkeys (Chan et al., 2014; Kocerha et al., 2013; Yang et al., 2008), lay the foundation for long-term assessment of the safety and efficacy of cell and gene therapies in HD monkey models.

EXPERIMENTAL PROCEDURES

In Vitro/In Vivo Neuronal Differentiation

NHP NPCs were seeded onto a P/L-coated glass chamber in differentiation medium (DMEM/F12 [Life Technologies], P/S [Invitrogen], 2 mM L-glutamine, 1 × N2 [Invitrogen], and 1 × B27 [Life Technologies]). At 4 days of neural induction, SHH (R&D Systems, 0.2 μg/ml) and FGF8 (R&D, 0.1 μg/ml) were added. At day 8, 200 mM ascorbic acid was added in combination with SHH and FGF8.

All protocols involving animal care and handling were approved by Emory University's Institutional Animal Care and Use Committee. For in vivo differentiation to the neuronal lineage, WT-2 NPCs and HD-14 NPCs were dissociated and suspended at 50,000 cells/μl in artificial cerebrospinal fluid solution. By stereotactic injection, the cell suspension was infused into the right and left hemispheres of the striatum. Further details are in the Supplemental Experimental Procedures.

Cell Stress and Apoptosis Assays

NPCs were treated with 5 mM H_2O_2 in culture medium for 24 hr. Caspase 3/7 activity was assessed using Muse Caspase-3/7 Kit (Millipore) according to the manufacturer's instructions. Cell counts were analyzed using Muse Cell Analyzer (Millipore). Effects of H_2O_2 were further assessed by TUNEL analysis as described in the Supplemental Experimental Procedures.

Statistical Analysis

For all comparisons one-way ANOVA analysis and Bonferonni post tests were performed using SPSS statistical software (IBM). Statistical significance was determined at $^*p < 0.05$ and $^{**}p < 0.001$.

SUPPLEMENTAL INFORMATION

Supplemental Information includes Supplemental Experimental Procedures, two figures, and two tables and can be found with this article online at http://dx.doi.org/10.1016/j.stemcr.2014.07.011.

ACKNOWLEDGMENTS

We thank Xiao-Jiang Li for providing mEM48 antibody, Gary Bassell for providing NR2A antibody, and Kiran Gill for assistance in FACS analysis. We also thank Cheryl Strauss for assistance in editing. YNPRC is supported by the Office of Research and Infrastructure Program (ORIP)/OD P51OD11132. K.P. and R.P. are supported by the Royal Golden Jubilee PhD program of Thailand Research Fund. R.L.C. is partly supported by NIH training grant to the Department of Human Genetics at Emory University (5T32MH879774). This study is supported by a grant awarded by the ORIP/NIH (OD010930), NINDS/NIH (NS084163), and ACTSI to A.W.S.C.

Received: February 3, 2014
Revised: July 22, 2014
Accepted: July 24, 2014
Published: September 4, 2014

REFERENCES

An, M.C., Zhang, N., Scott, G., Montoro, D., Wittkop, T., Mooney, S., Melov, S., and Ellerby, L.M. (2012). Genetic correction of Huntington's disease phenotypes in induced pluripotent stem cells. Cell Stem Cell *11*, 253–263.

Arrasate, M., Mitra, S., Schweitzer, E.S., Segal, M.R., and Finkbeiner, S. (2004). Inclusion body formation reduces levels of mutant huntingtin and the risk of neuronal death. Nature *431*, 805–810.

Boudreau, R.L., McBride, J.L., Martins, I., Shen, S., Xing, Y., Carter, B.J., and Davidson, B.L. (2009). Nonallele-specific silencing of mutant and wild-type huntingtin demonstrates therapeutic efficacy in Huntington's disease mice. Mol. Ther. *17*, 1053–1063.

Camnasio, S., Delli Carri, A., Lombardo, A., Grad, I., Mariotti, C., Castucci, A., Rozell, B., Lo Riso, P., Castiglioni, V., Zuccato, C., et al. (2012). The first reported generation of several induced pluripotent stem cell lines from homozygous and heterozygous Huntington's disease patients demonstrates mutation related enhanced lysosomal activity. Neurobiol. Dis. *46*, 41–51.

Chan, A.W.S., Cheng, P.-H., Neumann, A., and Yang, J.-J. (2010). Reprogramming Huntington monkey skin cells into pluripotent stem cells. Cell. Reprogram. *12*, 509–517.

Chan, A.W., Xu, Y., Jiang, J., Rahim, T., Zhao, D., Kocerha, J., Chi, T., Moran, S., Engelhardt, H., Larkin, K., et al. (2014). A two years longitudinal study of a transgenic Huntington disease monkey. BMC Neurosci. *15*, 36.

Cheng, P.-H., Li, C.-L., Chang, Y.-F., Tsai, S.-J., Lai, Y.-Y., Chan, A.W.S., Chen, C.-M., and Yang, S.-H. (2013). miR-196a ameliorates phenotypes of Huntington Disease in cell, transgenic mouse, and induced pluripotent stem cell models. Am. J. Hum. Genet. *93*, 306–312.

DiFiglia, M., Sapp, E., Chase, K.O., Davies, S.W., Bates, G.P., Vonsattel, J.P., and Aronin, N. (1997). Aggregation of huntingtin in neuronal intranuclear inclusions and dystrophic neurites in brain. Science *277*, 1990–1993.

Emborg, M.E., Liu, Y., Xi, J., Zhang, X., Yin, Y., Lu, J., Joers, V., Swanson, C., Holden, J.E., and Zhang, S.-C. (2013). Induced pluripotent stem cell-derived neural cells survive and mature in the nonhuman primate brain. Cell Rep. *3*, 646–650.

Grskovic, M., Javaherian, A., Strulovici, B., and Daley, G.Q. (2011). Induced pluripotent stem cells—opportunities for disease modelling and drug discovery. Nat. Rev. Drug Discov. *10*, 915–929.

Hashimoto, K., Shimada, H., Okada, Y., Ibata, K., Ebise, H., Ota, S.-i., Tomioka, I., Nomura, T., Maeda, T., Kohda, K., et al. (2012). Efficient derivation of multipotent neural stem/progenitor cells from non-human primate embryonic stem cells. PLoS One *7*, e49469.

HD iPSC Consortium (2012). Induced pluripotent stem cells from patients with Huntington's disease show CAG-repeat-expansion-associated phenotypes. Cell Stem Cell *11*, 264–278.

Johnson, C.D., and Davidson, B.L. (2010). Huntington's disease: progress toward effective disease-modifying treatments and a cure. Hum. Mol. Genet. *19* (R1), R98–R102.

Kocerha, J., Liu, Y., Willoughby, D., Chidamparam, K., Benito, J., Nelson, K., Xu, Y., Chi, T., Engelhardt, H., Moran, S., et al. (2013). Longitudinal transcriptomic dysregulation in the peripheral blood of transgenic Huntington's disease monkeys. BMC Neurosci. *14*, 88.

Koch, P., Opitz, T., Steinbeck, J.A., Ladewig, J., and Brüstle, O. (2009). A rosette-type, self-renewing human ES cell-derived neural stem cell with potential for in vitro instruction and synaptic integration. Proc. Natl. Acad. Sci. USA *106*, 3225–3230.

MacDonald, M.E., Ambrose, C.M., Duyao, M.P., Myers, R.H., Lin, C., Srinidhi, L., Barnes, G., Taylor, S.A., James, M., Groot, N., et al.; The Huntington's Disease Collaborative Research Group (1993). A novel gene containing a trinucleotide repeat that is expanded and unstable on Huntington's disease chromosomes. Cell *72*, 971–983.

Marco, S., Giralt, A., Petrovic, M.M., Pouladi, M.A., Martínez-Turrillas, R., Martínez-Hernández, J., Kaltenbach, L.S., Torres-Peraza, J., Graham, R.K., Watanabe, M., et al. (2013). Suppressing aberrant GluN3A expression rescues synaptic and behavioral impairments in Huntington's disease models. Nat. Med. *19*, 1030–1038.

McBride, J.L., Pitzer, M.R., Boudreau, R.L., Dufour, B., Hobbs, T., Ojeda, S.R., and Davidson, B.L. (2011). Preclinical safety of RNAi-mediated HTT suppression in the rhesus macaque as a potential therapy for Huntington's disease. Mol. Ther. *19*, 2152–2162.

Milnerwood, A.J., Gladding, C.M., Pouladi, M.A., Kaufman, A.M., Hines, R.M., Boyd, J.D., Ko, R.W.Y., Vasuta, O.C., Graham, R.K., Hayden, M.R., et al. (2010). Early increase in extrasynaptic NMDA receptor signaling and expression contributes to phenotype onset in Huntington's disease mice. Neuron *65*, 178–190.

Nicholas, C.R., Chen, J., Tang, Y., Southwell, D.G., Chalmers, N., Vogt, D., Arnold, C.M., Chen, Y.J., Stanley, E.G., Elefanty, A.G., et al. (2013). Functional maturation of hPSC-derived forebrain interneurons requires an extended timeline and mimics human neural development. Cell Stem Cell *12*, 573–586.

Nori, S., Okada, Y., Yasuda, A., Tsuji, O., Takahashi, Y., Kobayashi, Y., Fujiyoshi, K., Koike, M., Uchiyama, Y., Ikeda, E., et al. (2011). Grafted human-induced pluripotent stem-cell-derived neurospheres promote motor functional recovery after spinal cord injury in mice. Proc. Natl. Acad. Sci. USA *108*, 16825–16830.

Perrier, A., and Peschanski, M. (2012). How can human pluripotent stem cells help decipher and cure Huntington's disease? Cell Stem Cell *11*, 153–161.

Putkhao, K., Kocerha, J., Cho, I.-K., Yang, J., Parnpai, R., and Chan, A.W.S. (2013). Pathogenic cellular phenotypes are germline transmissible in a transgenic primate model of Huntington's disease. Stem Cells Dev. *22*, 1198–1205.

Snyder, B.R., Cheng, P.-H., Yang, J., Yang, S.-H., Huang, A.H.C., and Chan, A.W.S. (2011). Characterization of dental pulp stem/stromal cells of Huntington monkey tooth germs. BMC Cell Biol. *12*, 39.

Wang, C.E., Tydlacka, S., Orr, A.L., Yang, S.H., Graham, R.K., Hayden, M.R., Li, S., Chan, A.W.S., and Li, X.J. (2008). Accumulation of N-terminal mutant huntingtin in mouse and monkey models implicated as a pathogenic mechanism in Huntington's disease. Hum. Mol. Genet. *17*, 2738–2751.

Yang, S.-H., Cheng, P.-H., Banta, H., Piotrowska-Nitsche, K., Yang, J.-J., Cheng, E.C.H., Snyder, B., Larkin, K., Liu, J., Orkin, J., et al. (2008). Towards a transgenic model of Huntington's disease in a non-human primate. Nature *453*, 921–924.

Zhang, N., An, M.C., Montoro, D., and Ellerby, L.M. (2010). Characterization of human Huntington's disease cell model from induced pluripotent stem cells. PLoS Curr. *2*, RRN1193.

Stem Cell Reports, Volume *3*

Supplemental Information

Reversal of Cellular Phenotypes in Neural Cells Derived from Huntington's Disease Monkey-Induced Pluripotent Stem Cells

Richard L. Carter, Yiju Chen, Tanut Kunkanjanawan, Yan Xu, Sean P. Moran, Kittiphong Putkhao, Jinjing Yang, Anderson H.C. Huang, Rangsun Parnpai, and Anthony W.S. Chan

Supplemental Figures

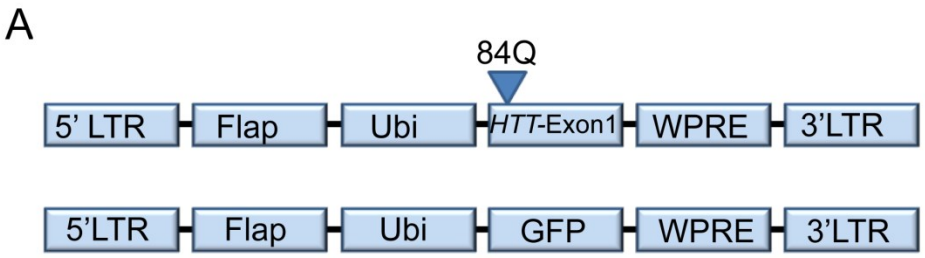

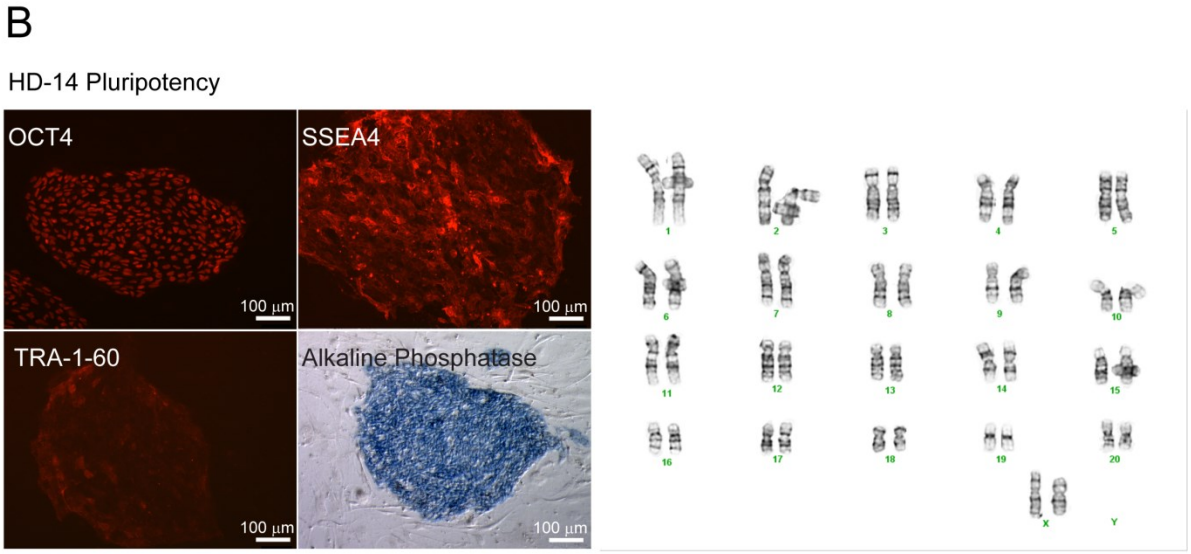

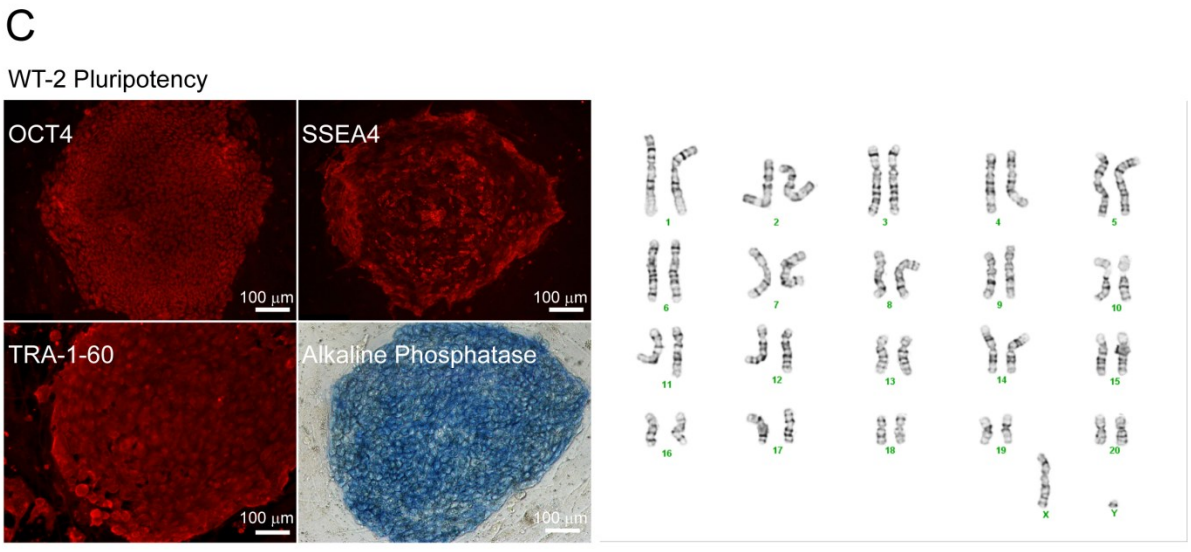

Figure S1. Generation of pluripotent stem cells from HD and WT monkeys, Related to Figure 1

(A) HD monkey cell lines are derived from HD monkeys carrying m*HTT* transgene. This schematic illustrates the lentiviral vector carrying exon 1 of the human *HTT* gene with expanded CAG repeats. Cells derived from HD monkeys also carry *GFP*. Both vectors are regulated by human poly-ubiquitin-C promoter. LTR, long terminal repeats; Flap, HIV-flap sequence; GFP, green florescent protein; *HTT*, human huntingtin exon 1; Ubi, ubiquitin promoter; WPRE, woodchuck post-transcriptional regulatory element (Yang et al., 2008).

(B) Reprogrammed HD-14 cells from HD monkey form colonies and express stem cell pluripotency markers OCT4, SSEA4, TRA-1-60, and alkaline phosphatase. G-banding analysis shows normal diploid karyotype. (42; XX)

(C) WT-2 from WT monkey ESCs form colonies and express stem cell pluripotency markers OCT4, SSEA4, TRA-1-60, and alkaline phosphatase. G-banding analysis shows normal diploid karyotype. (42; XY)

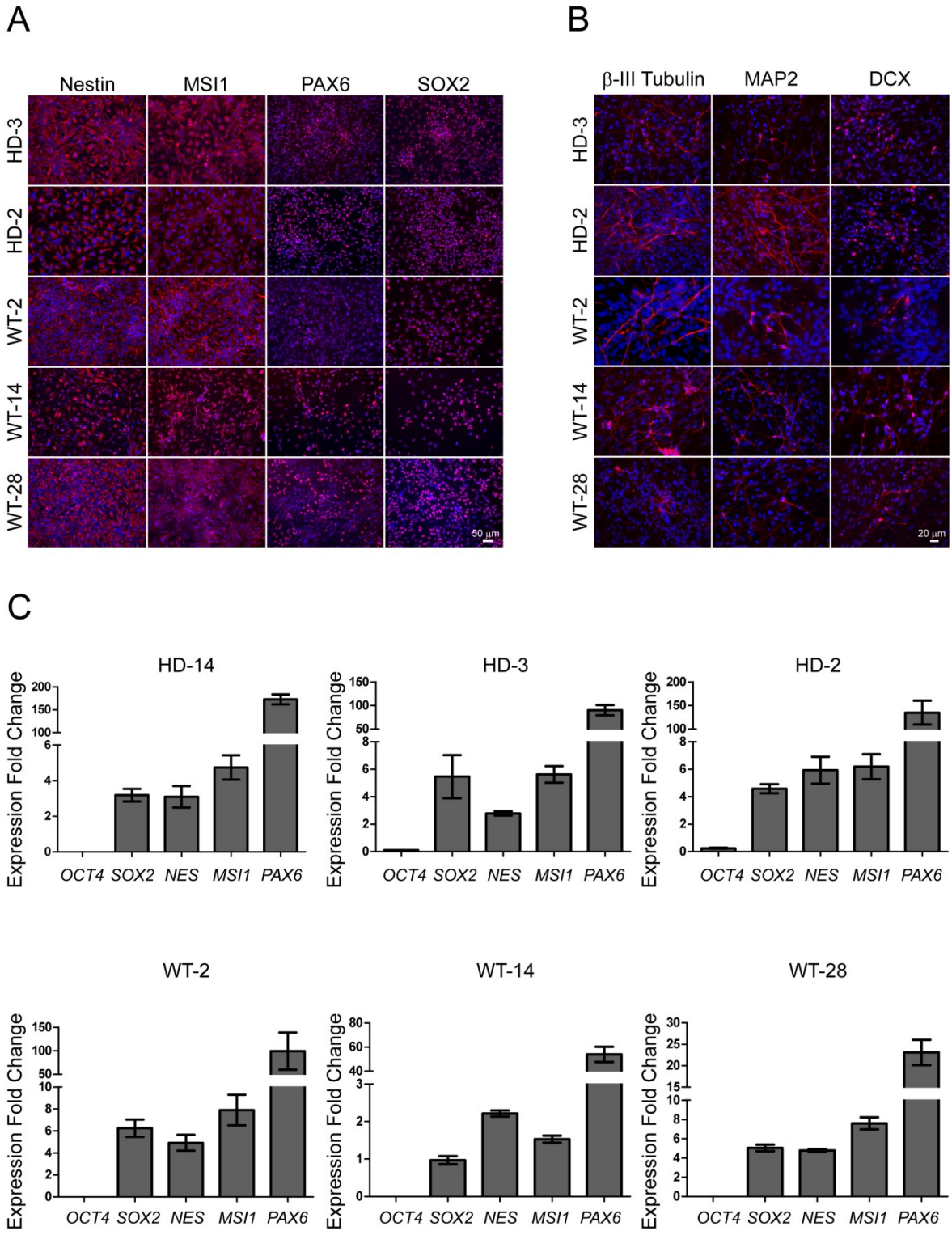
A
Nestin
MSI1
PAX6
SOX2
HD-3
HD-2
WT-2
WT-14
WT-28
50 μm
B
β-III Tubulin
MAP2
DCX
HD-3
HD-2
WT-2
WT-14
WT-28
20 μm
C
HD-14
HD-3
HD-2
WT-2
WT-14
WT-28
Expression Fold Change
OCT4 SOX2 NES MSI1 PAX6

Figure S2. Characterization of neural cells derived from HD and WT monkeys, Related to Figure 1

(A) Monkey NPCs except for HD-14 (shown in text) stained positively for Nestin, MSI1, PAX6, and SOX2 (red). Nuclear staining using Hoechst (blue).

(B) Monkey neural cells stained positive for β-III Tubulin (red), MAP2 (red), and DCX (red). Nuclear staining using Hoechst (blue).

(C) RT-qPCR shows elevated expression for NPC markers: *SOX2*, *NES* (Nestin), *MSI1*, and *PAX6*. Expression values were normalized to *GAPDH*. All graphs are relative to expression values in WT-2 ESCs and plotted as delta-delta CT method. Results were from three biological replicates. RT-qPCR samples run in duplicate. Data are represented as mean +/- SEM.

Table S1. Summary of HD and WT monkey cell lines included in this study, Related to Experimental Procedures

Cell Line	HD-2	HD-3	HD-14	WT-2	WT-14	WT-28
Phenotype	HD	HD	HD	WT	WT	WT
Source	ICM/ESC	Fibroblast	DPSC	ICM/ESC	Fibroblast	ICM/ESC
CAG size	29	72	27, 65	NP	NP	NP
Mutant *HTT* Expression	X	X	X	ND	ND	ND
ICC Characterization (Fig 1;S2)	X	X	X	X	X	X
RT-qPCR Characterization (Fig S2)	X	X	X	X	X	X
FACS Analysis (Fig 1)	X	X	X	X	X	X
HTT Western Blot	X	X	X	X	X	X
In Vitro Differentiation	X	X	X	X	X	X
In Vivo Differentiation	NP	NP	X	X	NP	NP
H_2O_2/TUNEL	X	X	X	X	X	X
Reference	Putkhao *et al*., 2012	Chan *et al*., 2010	Yang *et al*., 2008			

DPSC: Dental pulp stromal cells; ICM: Inner cell mass; ESC: embryonic stem cells; ICC: Immunocytochemistry; NP: Not performed; ND: Not detected

Table S2. Summary of FACS analysis in NPCs, Related to Figure 1

Cell Line	FACS Results (% Positive)			
	Nestin	**SOX2**	**PAX6**	**MSI1**
HD-14	99.3	99.1	91.1	99.8
HD-3	98.6	98.2	86.1	97.6
HD-2	99.6	99.5	94	98.6
WT-2	99.4	99.2	93.6	99.9
WT-14	99.8	99.8	91.1	99.8
WT-28	99.3	99.8	99.0	99.5

Supplemental Experimental Procedure

Reprogramming HD NHP iPSCs and Culture

HD monkeys were generated as described by Yang et al. Briefly, exon 1 of the human *HTT* gene with expanded CAG repeats was inserted into a lentiviral vector. An additional lentiviral vector carrying EGFP was created for co-infection. Both vectors were under the regulation of the human UBC promoter (Yang et al., 2008). HD dental pulp stromal cells and fibroblasts were harvested from the dental pulp and skin of HD monkeys as described previously (Chan et al., 2010; Snyder et al., 2011). Teeth germs/buds were recovered from a HD monkey euthanized soon after birth (Snyder et al., 2011). Harvested teeth germs/buds were then digested in 3 mg/ml collagenase type I and 4 mg/ml dispase (Invitrogen) for 1 hr at 37°C. Single cell suspension was filtered through a 70-μm cell strainer and then cultured in DPSC culture medium [a-MEM (Invitrogen) supplemented with 20% fetal bovine serum (FBS, Atlanta Biologicals, Lawrenceville, GA), 2 mM L-glutamine, and 1 x penicillin/streptomycin (P/S, Invitrogen)] at 37°C with 5% CO_2. Harvested DPSCs and fibroblasts were infected by retrovirus expressing rhesus macaque Oct4, Sox2, and Klf4. At approximately 2-3 weeks post-retroviral transfection, a primate ES cell-like colony was selected based on morphology and mechanically passaged onto mouse fetal fibroblast (MFF) feeder cells with primate ES media. Cell lines are further described in Table S1.

Cytogenetic Analysis/G-Banding Analysis

Cytogenetic analysis was performed by Cell Line Genetics, LLC (Madison, WI). A total of 20 metaphases were analyzed, and images were captured using the CytoVision® digital imaging system (Applied Imaging).

Derivation and Culture of NHP-NPCs

iPSCs were mechanically dissociated from MFF feeder and were cultured in low-attachment petri dishes supported by MFF-conditioned ES cell medium without bFGF (R&D). After 7 days ES cell medium was replaced with derivation medium [DMEM/F12 (with 1x N2 (Invitrogen), 4 ng/ml bFGF (R&D), 2 mM L-glutamine, and 1 x P/S (Invitrogen)]. During this period cells cultured without passage with medium refreshed every 2 days. After 7 days neurospheres were plated onto P/L-coated [1 μg/cm^2 laminin (Sigma) and 20 ug/mL Poly-L-ornithine (Sigma)] cell culture dishes and expanded in neural proliferation medium [Neurobasal medium (Life Technologies) supplemented with 1 x P/S (Invitrogen) and 1x B27 (Life Technologies), 2 mM L-glutamine, 20 ng/ml bFGF (R&D), and 10 ng/ml mLIF (Chemicon)]. After 7-10 days neural rosettes were manually picked and seeded onto a fresh P/L-coated cell culture dish.

In Vivo Neuronal Differentiation

For in vivo differentiation to the neuronal lineage, WT-2 NPCs and HD-14 NPCs were dissociated and suspended at 50,000 cells/μL in artificial cerebrospinal fluid solution. By stereotactic injection, cell suspension was infused into the right and left hemispheres of the striatum (Anterior-Posterior = +0.74, Medial-Lateral +/-1.7, dorsal/ventral = -3.8, relative to Bregma). Cell transplantation was performed in Fox River SCID® mice (CB17/lcr-, Charles River Laboratories).

Immunocytochemistry Antibodies

Fixed slides were incubated overnight at 4°C with primary antibodies, including Nestin (1:1000; Millipore), SOX2 (1:500; Stem Cell Technologies), MSI1 (1:500; Millipore), PAX6 (1:300; Covance, Atlanta, GA), GABA (1:300; Sigma), β-III Tubulin (1:300; Millipore), Tyrosine

Hydroxylase (TH; 1:100; Millipore), MAP2 (1:500, Millipore), NR2A (1:200, Millipore), GluR1 (1:300) and mGluR5 (1:500), and mEM48 (1:50). Secondary antibodies included Alexa Fluor 594 (1:1000; Life Technologies), Alexa Fluor 647 (1:500; Life Technologies), and Hoechst 33342 (5 mg/mL) for DNA staining. Samples were examined using a microscope (Olympus BX51) equipped with an epifluorescent device.

Histological Analysis

At 12.5, 15, and 16 weeks following transplantation, mice were perfused transcardially with PBS followed by 4% PFA prepared in PBS. Brains were dissected and postfixed in the 4% PFA overnight. Fixed brains were cryopreserved with 15% sucrose overnight and switched to 30% sucrose for 8 hr to reach equilibrium. The brains were then embedded in OCT compound and cryosectioned coronally to 30-μm thick slices. Free-floating brain slices were incubated in blocking buffer (5% serum and 2% BSA) for 30 min, and then incubated overnight at 4°C with primary antibodies, including DCX (1:500; AB18723, AbCam), NeuN (1:500; MAB377 Chemicon), GABA (1:300; A2052, Sigma), dopamine- and cAMP-regulated neuronal phosphoprotein (DARPP32; 1:200; 11365, Santa Cruz), GFAP (1:500; Chemicon), and mEM48 (1:50). Brain slices were washed with PBST (PBS + 0.2% Triton X-100) 3 times (10 min/time). Secondary antibodies (Alexa Fluor 594, A-21205; or Alexa Cy5, 81-6716) (1:500; Molecular Probes) were applied for 1.5 hr at room temperature. Slices were washed with PBST 2 times (10 min/time), and then incubated with Hoechst for 20 min. Subsequently, slices were mounted onto glass slides. Images were acquired using a Zeiss LSM 510 NLO META confocal microscope (Oberkochen, Germany).

Western Blot

Proteins were extracted using RIPA buffer and quantified by Bio-Rad DC Protein Assay (Pierce). Western blot was performed as described (Yang et al., 2008). Proteins were transferred to a PVDF membrane and probed with primary antibodies mEM48 (1:50), 1C2 (1:500), and γ-Tubulin (1:1000).

Fluorescence-Activated Cell Sorting (FACS) Analysis

Cells were dissociated using 1x Accutase (Life Technologies) and fixed in 1x BD FACS Permeabilizing Solution (BD Biosciences). Cells were washed following permeabilization. Cells were incubated with primary antibody for 1 hr, followed by 3 wash steps (5 min/wash) in 0.5% BSA/PBS. Cells were incubated with fluorochrome-conjugated secondary antibody for 1 hr in Falcon 5-mL round-bottom polystyrene tubes (BD Biosciences) and quantified on a FACSCalibur flow cytometer (BD Biosciences). All samples were gated to assess only single cells as determined by forward scatter area vs. side scatter area. Background fluorescence was subtracted using unlabeled cells, and channel compensation was performed using fluorochrome-labeled compensation beads (BD Biosciences). A total of 100,000 events were recorded. Quantification was analyzed using FlowJo analysis software (TreeStar).

Cell Stress and TUNEL Assays

Hydrogen Peroxide (H_2O_2): NPCs were treated with 5 mM H_2O_2 in culture medium for 24 hr. Following incubation cells were harvested and stained to assess caspase 3/7 activity using Muse™ Caspase-3/7 Kit (Millipore) according to the manufacturer's instructions. Cell counts were analyzed using Muse Cell Analyzer (Millipore).

TUNEL: Effects of H_2O_2 were further assessed by TUNEL analysis. Samples were prepared on P/L-coated coverslips. Following H_2O_2 treatment for 24 hr, samples were fixed in 4% PFA and

stained using an In Situ Cell Death Detection Kit (Roche) to quantify the percentage of TUNEL-positive cells. For 3 biological replicates, 6 images were taken randomly and quantified using CellSens software (Olympus).

Cytotoxicity Assay

Monkey neural cells were differentiated for 21 days and then treated with 10 μM memantine (Sigma) for 24 hr. Vybrant Cytotoxicity Assay Kit (Life Technologies) was used according to the manufacturer's instructions to assess cytotoxicity.

Real-Time Quantitative PCR

Total RNA from cell samples was prepared using TRIzol® (Life Technologies) followed by reverse transcription using a RNA-to-cDNA kit (Applied Biosystems). RT-qPCR was performed using Gene Expression Master Mix (Applied Biosystems) and TaqMan® gene expression primers on CFX96 Real-Time Detection System (Bio-Rad). Primer sequences are listed in Supplemental Methods.

RT-qPCR TaqMan® Primers

Gene Symbol	TaqMan® Primer Context Sequence
GAPDH	TCCAGGAGCGAGATCCCTCCAAAAT
MSI1	TTTGAGCAGTTTGGGAAGGTGGACG
NES	CCACGTACAGGACCCTCCTGGAGGC
PAX6	ATGCAGAACAGTCACAGCGGAGTGA
POU5F1 (OCT4)	CCCTGGGGGTTCTATTTGGGAAGGT
SOX2	GGCCCCGGCGGAAAACCAAGACGCT

RT-qPCR SYBR Primers

Gene Symbol	Forward Primer	Reverse Primer
HTT Exon 1	GCGACCCTGGAAAAGCTGAT	CTGCTGCTGCTGGAAGGACT
Ubiquitin C	CCACTCTGCACTTGGTCCTG	CCAGTTGGGAATGCAACAACTTTA